Energy & Environmental Science

RSC Publishing

COMMUNICATION

View Article Online
View Journal | View Issue



# Depleted hole conductor-free lead halide iodide heterojunction solar cells

Cite this: *Energy Environ. Sci.*, 2013, **6**, 3249

Received 7th July 2013
Accepted 4th September 2013

DOI: 10.1039/c3ee42282h

www.rsc.org/ees

Waleed Abu Laban and Lioz Etgar*

**Lead halide perovskite is an excellent candidate for use as a light harvester in solar cells. Our work presents a depleted hole conductor free $CH_3NH_3PbI_3/TiO_2$ heterojunction solar cell using a thick $CH_3NH_3PbI_3$ film. The $CH_3NH_3PbI_3$ formed large crystals which function simultaneously as light harvesters and as hole transport materials. We performed capacitance voltage measurements, which show a depletion region which extends to both n and p sides. The built-in field of the depletion region assists in the charge separation and suppresses the back reaction of electrons from the $TiO_2$ film to the $CH_3NH_3PbI_3$ film. This depleted hole conductor free $CH_3NH_3PbI_3/TiO_2$ heterojunction solar cell provides a power conversion efficiency of 8% with a current density of 18.8 mA $cm^{-2}$, the highest efficiency achieved to date for perovskite based solar cells without a hole conductor.**

### Broader context

Finding solutions for alternative energy is currently a leading research area and will remain so for the foreseeable future, when photovoltaic (PV) is one of the key technologies towards a sustainable energy supply. Recent discoveries revealed a breakthrough in the field using inorganic–organic hybrid layers named perovskites. The organic–inorganic arrangement is self-assembled as alternate layers, being a simple low cost procedure. These organic–inorganic hybrids promise a few benefits that cannot be encountered by the separate constituents. Latest reports showed high efficiencies for the perovskite based solar cells when using various hole transport materials (HTM). However, the HTM can cause oxidation and infiltration problems into the porous metal oxide in addition to the increase in the solar cell cost. In this work, we present a high efficiency $CH_3NH_3PbI_3$ heterojunction solar cell, which can function simultaneously as a light harvester and as a hole transport material. We performed capacitance voltage measurements and observed the doping density of the $CH_3NH_3PbI_3$ and the depletion layer which extends to both sides, the mesoporous $TiO_2$ film and the $CH_3NH_3PbI_3$ layer. This depleted hole conductor free $CH_3NH_3PbI_3/TiO_2$ heterojunction solar cell gives a PCE of 8%, the highest efficiency achieved so far for perovskite based solar cells without a hole conductor.

## Introduction

Layered perovskites are attracting increased attention due to their technological importance in solar energy conversion. Latest reports show promising photovoltaic performance when using perovskites as sensitizers in solar cells.

The basic layered perovskite structures[1] are $(R–NH_3)_2MX_4$ and (NH–R–NH)MX (X = $Cl^{-1}$, $Br^{-1}$, or $I^{-1}$). The M cation is generally a divalent metal that satisfies charge balancing and adopts an octahedral anion coordination. The inorganic layers consist of sheets of corner-sharing metal halide octahedra.

The layered perovskite has a large absorption coefficient, high carrier mobility, direct band gap and high stability.[2–4] These properties make it attractive for use in optoelectronic applications. The electronic coupling between the inorganic sheets and their distance from each other control the electronic properties of these layered materials.

Several reports used $CH_3NH_3PbI_3$ perovskite nanocrystals as sensitizers with a liquid electrolyte.[5–7] The performance of these systems rapidly declined due to the dissolution of the perovskite. $CsSnI_3$ was used as a solid hole conductor in solid state solar cells, achieving a power conversion efficiency (PCE) of 8.5%.[8] Further progress was achieved by Kim *et al.* who reported on a PCE of 9.7%[9] and Heo *et al.* who reported on a PCE of 12%.[10] In these reports, the authors used the Spiro-MeOTAD and a poly-triarylamine (PTAA) polymer as the hole conductor, respectively; their device architecture was more like a pillar structure with small $CH_3NH_3PbI_3$ crystalline domains. In addition to these achievements, Lee *et al.* have reported on a PCE of 10.9% using the spiro as a hole conductor.[11] In this work, an open circuit voltage of more than 1 V was presented, even though the energy band gap is around 1.5 eV. The same authors reported on a low-temperature processed meso-superstructure of thin-film perovskite solar cells achieving a PCE of 12.3%, when they reduced the temperature processing of the $Al_2O_3$ from 500 °C to 150 °C.[12] The use of $CH_3NH_3PbI_3$ as both a light harvester and a hole conductor was recently reported achieving

*The Institute of Chemistry, The Casali Center of Applied Chemistry, The Hebrew University of Jerusalem, Israel. E-mail: lioz.etgar@mail.huji.ac.il*

a PCE of 5.5%.[13] In addition, a high open circuit voltage of 1.15 V was achieved using a $CH_3NH_3PBr_3$ sensitized hybrid device with poly[*N*-9-hepta-decanyl-2,7-carbazole-*alt*-3,6-bis-(thiophen-5-yl)-2,5-dioctyl-2,5-di hydropyrrolo[3,4-]pyrrole-1,4-dione] (PCBTDPP) as the hole transport material.[14] The deposition of $CH_3NH_3PbI_3$ on rutile $TiO_2$ nanorods was demonstrated having a PCE of 9.4%.[15] More recently, a two-step deposition technique of the $CH_3NH_3PbI_3$ on the mesoporous $TiO_2$ showed an impressive PCE of 15%.[16]

Here, we report on a depleted hole conductor free $CH_3NH_3PbI_3/TiO_2$ heterojunction solar cell. A thick $CH_3NH_3PbI_3$ film was deposited on top of the mesoporous $TiO_2$, the $CH_3NH_3PbI_3$ has large crystals which function as light harvesters and hole transport materials at the same time. We performed capacitance voltage measurements and observed the doping density of the $CH_3NH_3PbI_3$ and the depletion layer which extends to both sides, the mesoporous $TiO_2$ film and the $CH_3NH_3PbI_3$ layer. This depleted hole conductor free $CH_3NH_3PbI_3/TiO_2$ heterojunction solar cell gives a PCE of 8% with a current density of 18.8 mA $cm^{-2}$, the highest efficiency achieved so far for perovskite based solar cells without hole conductors.

## Experimental

### Method and device fabrication

$CH_3NH_3I$ was synthesized by reacting 30 mL of methylamine (40% in methanol, TCI) and 32.3 mL of hydroiodic acid (57 wt% in water, Aldrich) in a 250 mL round bottom flask at 0 °C for 2 h with stirring. The precipitate was recovered by putting the solution on a rotavap and carefully removing the solvents at 50 °C. The yellowish raw product of methylammonium iodide ($CH_3NH_3I$) was washed with diethyl ether by stirring the solution for 30 min, a step which was repeated three times, and then the $CH_3NH_3I$ was finally recrystallized from a mixed solvent of diethyl ether and ethanol. After filtration, the solid was collected and dried at 60 °C in a vacuum oven for 24 h.

**Device fabrication.** A $SnO_2$:F conducting glass substrate (15 Ω $cm^{-1}$, Pilkington) was immersed in 40 mM $TiCl_4$ aqueous solution for 30 min at 70 °C and washed with distilled water and ethanol, followed by annealing at 500 °C for 30 min in air.

22 nm $TiO_2$ nanoparticle films of ~0.3 μm thickness were spin coated onto this substrate. The $TiO_2$ layer was annealed at 500 °C for 30 min in air. The substrate was then immersed again in 40 mM $TiCl_4$ aqueous solution for 30 min at 70 °C and washed with distilled water and ethanol, followed by annealing at 500 °C for 30 min in air.

The synthesis of $CH_3NH_3PbI_3$ on the $TiO_2$ surface was carried out by dropping a 40 wt% precursor solution of equimolar $CH_3NH_3I$ and $PbI_2$ in γ-butyrolactone onto the $TiO_2$ film.[7] Film formation was induced by spin coating (2000 rpm, 30 s) the $CH_3NH_3PbI_3$ twice under glove box conditions. In the first spin, the $CH_3NH_3PbI_3$ was dissolved in γ-butyrolactone, while in the second spin, it was dissolved in dimethylformamide. The film coated onto the $TiO_2$ changed color on drying at room temperature, indicating the formation of $CH_3NH_3PbI_3$ in the solid state. The $CH_3NH_3PbI_3$ film was annealed under argon for 15 min at 100 °C.

Finally, the counter electrode was deposited by thermal evaporation of gold under a pressure of $5 \times 10^{-5}$ Torr. The active area was 0.09 $cm^2$. After the preparation, the cells were exposed to air.

**Extra high resolution scanning electron microscopy.** Magellan XHR SEM was performed with FEI (Field Emission Instruments), The Netherlands. The measurement conditions were 5 kV at a magnification of 100 000.

**X-ray diffraction.** X-ray powder diffraction measurements were performed in grazing incidence X-ray diffraction (GIXRD) mode on the D8 Advance diffractometer (Bruker AXS, Karlsruhe, Germany) with a goniometer radius of 217.5 mm, a secondary graphite monochromator, 2° Soller slits and a 0.2 mm receiving slit. XRD patterns within the range 5° to 60° 2$\theta$ were recorded at room temperature using CuKα radiation ($\lambda = 1.5418$ Å) with the following measurement conditions: tube voltage of 40 kV, tube current of 40 mA, step-scan mode with a step size of 0.02° 2$\theta$ and counting time of 1–3 s per step. The value of the grazing incidence angle was 2.5°.

### Photovoltaic characterization

Photovoltaic measurements employed on a New Port system, an Oriel *I–V* test station using an Oriel Sol3A simulator. The solar simulator is class AAA for spectral performance, uniformity of irradiance, and temporal stability.

The solar simulator is equipped with a 450 W xenon lamp. The output power is adjusted to match AM 1.5 global sunlight (100 mW $cm^{-2}$). The spectral match classifications are IEC 60904-9 2007, JIC C 8912, and ASTM E927-05. *I–V* curves were obtained by applying an external bias to the cell and measuring the generated photocurrent with a Keithley model 2400 digital source meter. The voltage step and delay time of photocurrent were 10 mV and 40 ms, respectively.

Oriel IQE-200 was used to determine the monochromatic incident photon-to-electric current conversion efficiency. Under full computer control, light from a 150 W xenon arc lamp was focused through a monochromator in the 300–1800 nm wavelength range onto the photovoltaic cell under test. The monochromator was incremented through the visible spectrum to generate the IPCE ($\lambda$) as defined by IPCE ($\lambda$) = 12 400 ($J_{sc}/\lambda\varphi$), where $\lambda$ is the wavelength, $J_{sc}$ is the short-circuit photocurrent density (mA $cm^{-2}$), and $\varphi$ is the incident radiative flux (mW $cm^{-2}$). Photovoltaic performance was measured by using a metal mask with an aperture area of 0.09 $cm^2$.

**Capacitance voltage measurements.** The measurements were performed using a Metrohm Autolab system, equipped with a PGTSTAT302N potentiostat instrument. The frequency was 1 kHz at bias potentials between 0 and 0.8 V.

## Results and discussion

The synthesis of $CH_3NH_3PbI_3$ and the deposition on the mesoporous $TiO_2$ film were carried out by twice spin coating a 40 wt % precursor solution of $CH_3NH_3I$ and $PbI_2$ in γ-butyrolactone and dimethylformamide. After drying at room temperature, the film coated onto the $TiO_2$ darkened in color, indicating the

 

formation of $CH_3NH_3PbI_3$ in the solid state. The ionic and covalent interactions between the metal cations and the halogen anions create inorganic octahedra, while the cationic alkylammonium head groups provide charge balance to the structure.

A scheme of the depleted $CH_3NH_3PbI_3/TiO_2$ heterojunction solar cell on a 300 nm mesoporous $TiO_2$ film is shown in Fig. 1A. The mesoporous $TiO_2$ was coated with the $CH_3NH_3PbI_3$ layer, while gold was evaporated as the back contact of the device. Fig. 1B shows a schematic energy level diagram of the depleted $CH_3NH_3PbI_3/TiO_2$ heterojunction solar cell.

The $CH_3NH_3PbI_3/TiO_2$ heterojunction solar cell shows a depletion layer due to the charge transfer from the electron accepting contact to the $CH_3NH_3PbI_3$ layer. On illumination, the $CH_3NH_3PbI_3$ perovskite should absorb the light, and as a result electrons are transferred from the $CH_3NH_3PbI_3$ perovskite to the $TiO_2$ and holes are transported to the gold contact.

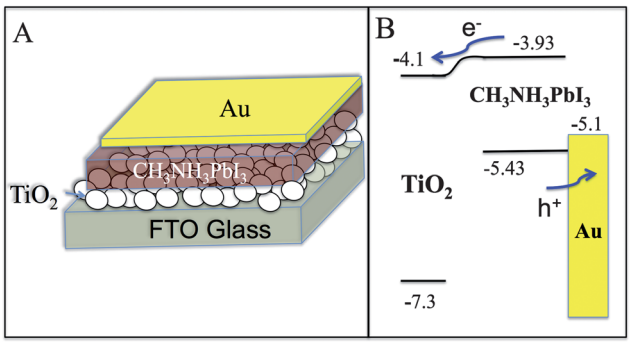


**Fig. 1** (A) Schematic illustration of the $CH_3NH_3PbI_3/TiO_2$ heterojunction solar cell. (B) Energy level diagram of the discussed solar cell which shows the charge separation process. The positions of the energy levels are according to ref. 13.

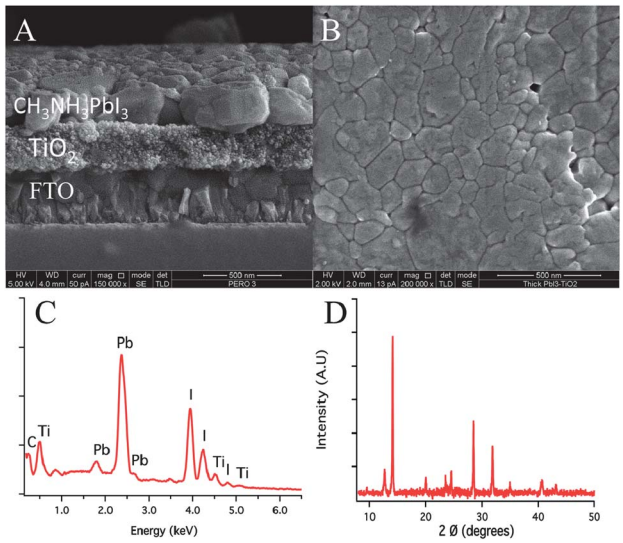


**Fig. 2** (A) HR-SEM cross section of the $CH_3NH_3PbI_3/TiO_2$ heterojunction solar cell. (B) HR-SEM top view of the $CH_3NH_3PbI_3$ perovskite film deposited on the $TiO_2$ film. (C) EDS spectra of the $CH_3NH_3PbI_3$ layer which is shown in the HR-SEM image, presented in (B). (D) XRD pattern of the $CH_3NH_3PbI_3$ on the mesoporous $TiO_2$ film.

Fig. 2B shows a high resolution scanning electron microscopy (HR-SEM) top view image of the $CH_3NH_3PbI_3$ perovskite film on the $TiO_2$ film where the crystal domains of the $CH_3NH_3PbI_3$ can be observed. The cross section of the photovoltaic device is shown in Fig. 2A. The mesoporous $TiO_2$ film is 300 nm thick while the $CH_3NH_3PbI_3$ perovskite film is clearly seen on top of the $TiO_2$ film with a wide range of crystal sizes between 50 and 300 nm. The thickness of the $CH_3NH_3PbI_3$ perovskite is about 300 nm. The energy dispersive spectroscopy (EDS) spectrum of the $CH_3NH_3PbI_3$ deposited on top of the mesoporous $TiO_2$ is shown in Fig. 2C; all elements can be observed.

Fig. 2D shows the XRD pattern of the $CH_3NH_3PbI_3$ on the mesoporous $TiO_2$ film. The peaks of the $CH_3NH_3PbI_3$ on the $TiO_2$ show the crystalline form of the $CH_3NH_3PbI_3$ and they match closely with the peaks reported in ref. 7 and 10.

Fig. 3A shows the $J$–$V$ spectra of the $CH_3NH_3PbI_3/TiO_2$ heterojunction solar cells. The cell gives a $J_{sc}$ of 18.8 mA cm$^{-2}$, a FF of 0.6 and a $V_{oc}$ of 0.712 V reaching an impressive power conversion efficiency of 8% under 1 sun illumination.

The incident photon to current efficiency (IPCE) spectra specifies the ratio of extracted electrons to incident photons at a given wavelength. The IPCE spectrum (Fig. 3B) is plotted as a function of wavelength of the light. The $CH_3NH_3PbI_3/TiO_2$ heterojunction solar cell has a good response from the visible region until 800 nm, achieving around 80% in the 400–600 nm range. Integration over the IPCE spectra gives 18 mA cm$^2$, which is in good agreement with the current density calculated from the current–voltage measurements.

Fig. 3C shows the reproducibility of performance for the $CH_3NH_3PbI_3/TiO_2$ heterojunction solar cells. More than 50% of the cells show efficiencies above 7.5%, while more than 10% show efficiencies above 7.8%. The average power conversion efficiency is 7.15%.

To further understand the operation mechanism of the $CH_3NH_3PbI_3/TiO_2$ heterojunction solar cell, capacitance voltage measurements were performed. The capacitance arises from the depletion layer due to the charge transfer from $TiO_2$ to the $CH_3NH_3PbI_3$ layer.

To estimate the depletion layer and the doping density, we preformed Mott–Schottky analysis[17] on the lead iodide/$TiO_2$ heterojunction solar cell. The results are presented in Fig. 4A.

The junction capacitance (eqn (1)) is calculated from the depletion approximation,[18] which implies that there are no free carriers in the space charge region at the junction under investigation.

$$\frac{1}{C^2} = \frac{2}{\varepsilon\varepsilon_0 q A^2 N}(V_{bi} - V) \quad (1)$$

where $C$ is the measured capacitance, $A$ is the active area, $V$ is the applied bias, $\varepsilon$ is the static permittivity, $\varepsilon_0$ is the permittivity of free space, $q$ is the elementary charge and $N$ is the doping density of the donor.

The static permittivity of $CH_3NH_3PbI_3$ was measured and calculated to be 30 according to ref. 19 and 20. The slope of $1/C^2$ *vs.* $V$ in the linear regime was $2.71 \times 10^{15}$ F$^{-2}$ V$^{-1}$, from which the net doping density in the $CH_3NH_3PbI_3$ film is found to be $2.14 \times 10^{17}$ cm$^{-3}$.

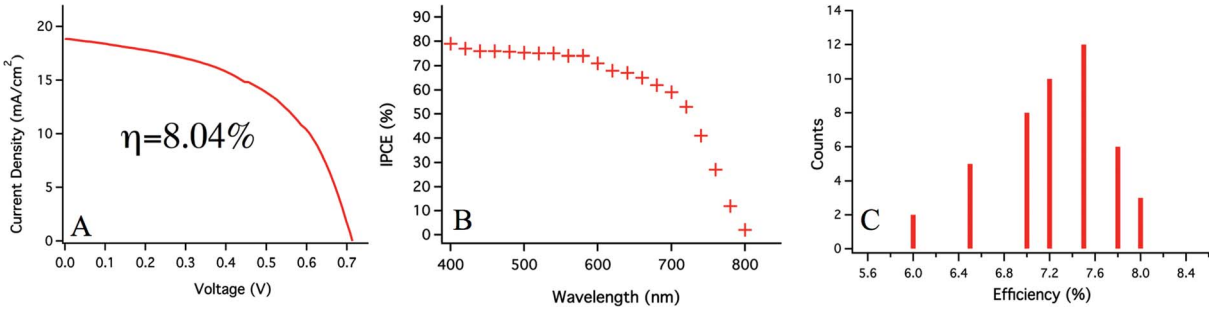


**Fig. 3** (A) *J–V* characteristics of the depleted lead iodide/$TiO_2$ heterojunction solar cell. (B) IPCE of the lead iodide/$TiO_2$ heterojunction solar cell. (C) Histogram of the efficiencies for 40 cells of the lead iodide/$TiO_2$ heterojunction solar cells.

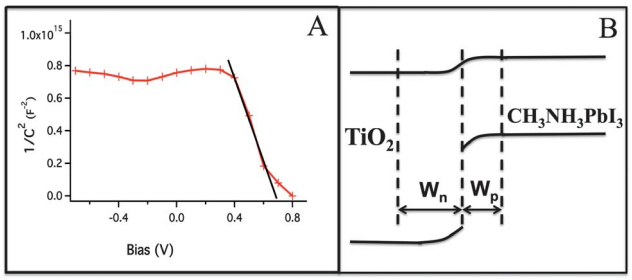


**Fig. 4** (A) Mott–Schottky analysis at 1 kHz for the $CH_3NH_3PbI_3/TiO_2$ heterojunction solar cell. A linear fit (shown as the black line) shows that the built-in potential is 0.67 V, and the approximate value for the doping density in the $CH_3NH_3PbI_3$ layer is $2.14 \times 10^{17}$ $cm^{-3}$. (B) Schematic band bending diagram. The depletion width on the n-side ($W_n$) was calculated to be 162 nm and on the p-side ($W_p$) was calculated to be 75 nm.

In addition, the built-in potential can be calculated using the intercept of the linear regime with the *x*-axis of the Mott–Schottky plot, which is equal to 0.67 V, which is in good agreement with the $V_{oc}$ of the device.

This is a direct signature of the presence of a built-in field that efficiently drives the separation of photo-generated carriers. Moreover, this built-in field of the depletion region suppressed the back reaction of electrons from the $TiO_2$ film to the $CH_3NH_3PbI_3$ film.

The depletion width is calculated according to:[21]

$$W_{p,n} = \frac{1}{N_{a,d}} \sqrt{\frac{2\varepsilon V_{bi}}{q\left(\frac{1}{N_a + N_d}\right)}} \quad (2)$$

where $N_a$ and $N_d$ are the doping densities of the acceptor and the donor, respectively. Literature values for doping density in nanoporous $TiO_2$ start at $N_a = 1 \times 10^{16}$ $cm^{-3}$.[22–24] Using eqn (2), the depletion width on the n-side and on the p-side was calculated. The depletion width on the n-side was calculated to be 162 nm and on the p-side 75 nm. The schematic bend banding diagram is shown in Fig. 4B. According to Fig. 2A, the thickness of the $CH_3NH_3PbI_3$ layer and the thickness of the $TiO_2$ film are *ca.* 350 nm and *ca.* 300 nm, respectively. This suggests that half of the mesoporous $TiO_2$ film is depleted, while more than a fifth of the $CH_3NH_3PbI_3$ layer is depleted. Importantly, the built-in field in the depletion region assists in the charge separation of the photo-generated carriers. Consequently, some of the photo-generated carriers in the $CH_3NH_3PbI_3$ layer have to transport through the film to the depletion layer, while some of them have to transport to the counter electrode.

Future work will concentrate on extending the depletion region in the $CH_3NH_3PbI_3$ film, in order to minimize the transport distance for the photo-generated carriers.

## Conclusions

This paper presents high efficiency $CH_3NH_3PbI_3/TiO_2$ heterojunction solar cells; the $CH_3NH_3PbI_3$ simultaneously functions as a light harvester and a hole conductor. The photovoltaic performance showed a power conversion efficiency of 8% under 1 sun illumination. Mott–Schottky analysis shows a depletion region which extends to both n and p sides. The built-in field of the depletion region assists in the charge separation and suppresses the back reaction of electrons from the $TiO_2$ film to the $CH_3NH_3PbI_3$ film. The research sheds more light on the operation mechanism in this hole conductor free $CH_3NH_3PbI_3/TiO_2$ heterojunction solar cell.

## Acknowledgements

We would like to thank Dr Vladimir Uvarov and Ms Evgenia Blayvas from the Harvey M. Krueger Center for Nanoscience and Nanotechnology at the Hebrew University for the XRD and the HR-SEM measurements, respectively.

## Notes and references

1 D. B. Mitzi, *Synthesis, Structure, and Properties of Organic–Inorganic Perovskites and Related Materials, in Progress in Inorganic Chemistry*, John Wiley & Sons, Inc., New York, 1999, vol. 48, p. 1.
2 A. Kojima, M. Ikegami, K. Teshima and T. Miyasaka, *Chem. Lett.*, 2012, **41**, 397.
3 C. R. Kagan, D. B. Mitzi and C. D. Dimitrakopoulos, *Science*, 1999, **286**, 945.
4 D. B Mitzi, C. A. Field, Z. Schlesinger and R. B. Laibowitz, *J. Solid State Chem.*, 1995, **114**, 159.
5 A. Kojima, K. Teshima, Y. Shirai and T. Miyasaka, *J. Am. Chem. Soc.*, 2009, **131**, 6050–6051.
6 J. HyoekIm, J. Chung, S.-J. Kim and N.-G. Park, *Nanoscale Res. Lett.*, 2012, **7**, 353.

 

7 J. HyoekIm, C.-R. Lee, J.-W. Lee, S.-W. Park and N.-G. Park, *Nanoscale*, 2011, **3**, 4088.
8 I. Chung, B. Lee, J. He, R. P. H. Chang and M. G. Kanatzidis, *Nature*, 2012, **485**, 486–489.
9 H.-S. Kim, C.-R. Lee, J.-H. Im, K.-B. Lee, T. Moehl, A. Marchioro, S.-J. Moon, R. H. Baker, J. H. Yum, J. E. Moser, M. Grätzel and N.-G. Park, *Sci. Rep.*, 2012, **2**, 591.
10 J. Hyuck Heo, S. HyukIm, J. Hong Noh, T. N. Mandal, C.-S. Lim, J. A. Chang, Y. Hui Lee, H.-j. Kim, A. Sarkar, M. K. Nazeeruddin, M. Grätzel and S. Il Seok, *Nat. Photonics*, 2013, **7**, 486–491.
11 M. Lee, M. J. Teuscher, T. Miyasaka, T. N. Murakami and H. J. Snaith, *Science*, 2012, **338**, 643–644.
12 B. M. James, M. L. Michael, H. Andrew and H. J. Snaith, *Energy Environ. Sci.*, 2013, **6**, 1739.
13 L. Etgar, P. Gao, Z. Xue, Q. Peng, A. K. Chandiran, B. Liu, M. K. Nazeeruddin and M. Grätzel, *J. Am. Chem. Soc.*, 2012, **134**, 17396–17399.
14 B. Cai, Y. Xing, Z. Yang, W.-H. Zhang and J. Qiu, *Energy Environ. Sci.*, 2013, **6**, 1480.
15 H.-S. Kim, J.-W. Lee, N. Yantara, P. P. Boix, S. A. Kulkarni, S. Mhaisalkar, M. Grätzel and N.-G. Park, *Nano Lett.*, 2013, **13**, 2412–2417.
16 J. Burschka, N. Pellet, S.-J. Moon, R. H. Baker, P. Gao, M. K. Nazeeruddin and M. Grätzel, *Nature*, 2013, **499**, 316.
17 W. Schottky, Vereinfachte und ErweiterteTheorie der Randschicht-Gleichrichter, *Z. Phys.*, 1942, **118**, 539–592.
18 J. P. Clifford, K. W. Johnston, L. Levina and E. H. Sargent, *Appl. Phys. Lett.*, 2007, **91**, 253117.
19 A. Poglitsch and D. Weber, *J. Chem. Phys.*, 1987, **87**, 6373–6378.
20 T. Baikie, Y. Fang, J. M. Kadro, M. Schreyer, F. Wei, S. G. Mhaisalkar, M. Graetzel and T. J. White, *J. Mater. Chem. A*, 2013, **1**, 5628–5641.
21 J. M. Luther, M. Law, M. C. Beard, Q. Song, M. O. Reese, R. J. Ellingson and A. J. Nozik, *Nano Lett.*, 2008, **8**(10), 3488–3492.
22 B. O'Regan, J. Moser, M. Anderson and M. Graetzel, *J. Phys. Chem.*, 1990, **94**, 8720–8726.
23 S. Nakade, Y. Saito, W. Kubo, T. Kanzaki, T. Kitamura, Y. Wada and S. Yanagida, *Electrochem. Commun.*, 2003, **5**, 804–808.
24 A. Zaban, A. Meier and B. A. Gregg, *J. Phys. Chem. B*, 1997, **101**, 7985–7990.